

# **Development of ZnO-GaN hybrid spin LED**

Contract No. FA9550-05-C-0042

Final Technical Report  
October 15, 2007

Ian Ferguson  
Georgia Institute of Technology  
School of Electrical and Computer Engineering  
Atlanta, GA 30332-0250  
Phone: (404) 385-2885  
Fax: (404) 385-2886  
E-mail: [ianf@ece.gatech.edu](mailto:ianf@ece.gatech.edu)

## **ABSTRACT**

This report describes the development of a hybrid LED with spin polarized emission. The objectives of this effort were to integrate doped ZnO thin films into nitride LED structures to produce spin polarized light emission in the visible portion of the spectrum. These devices have military and commercial applications ranging from data storage to optical transmission networks. The work was successful, with full characterization of the magnetic properties of the doped ZnO and demonstration of hybrid diodes containing these materials.

## **1. Introduction**

Zinc oxide has a room temperature band gap of  $3.37 \text{ eV}^1$  and an exciton binding energy of  $60 \text{ meV}^2$ . ZnO in pure form has optical transparency ranging between 380 and 2500nm. ZnO has shown a wide range of technological applications such as transparent conducting electrodes in solar cells, flat panel displays, surface acoustic wave devices and chemical sensors<sup>3</sup>. There has been growing interest in ZnO recently due to its large band gap, which results in potential applicability to optoelectronic devices such as light emitting and laser diodes, which cover a wide visible range from red to blue. The exciton binding energy of ZnO is twice that of GaN ( $28 \text{ meV}$ )<sup>4</sup>, and due to such large binding energy the exciton remains dominant in optical processes in ZnO even above room temperature, giving an advantage over GaN for exciton-related device applications. ZnO can be grown in high quality, bulk form (currently available from Cermet, Inc. in 50 mm diameter)<sup>5</sup> and is relatively inexpensive. Additionally, ZnO doped with transition metals has become more attractive in the field of diluted magnetic semiconductors<sup>6</sup>. Compared to other DMS materials, ZnO has the following advantages<sup>7</sup> 1. ZnO has a large electron mass,  $\sim 0.3 m_e$ , is expected to exhibit a strong magnetic interaction between mobile carriers and localized magnetic ions. 2. ZnO is transparent in the visible region due to its large band gap making transparent magnets feasible. 3. Since ZnO is one of the promising UV laser devices<sup>8</sup>, integrating magnetic and optical hybrid devices based on single compound is possible. It has been predicted that Mn doped ZnO will be room temperature transparent ferromagnetic if the system is co-doped for p-type. Sato et al<sup>9</sup> predicted by band calculation that ZnO doped with V, Cr, Fe, Co and Ni can also be ferromagnetic at room temperature. With the help of Airforce and Missile Defense Agency and SBIR/STTRs Cermet is rapidly closing the gap in the development of pure and doped ZnO bulk substrates and thin films for various potential applications. We have chosen ZnO for this effort, as Cermet has vast experience in growing bulk and thin films of ZnO. Additionally, Cermet is a world leader in the growth of ZnO bulk material for homoepitaxial substrates. For this work, Cermet, Inc is teaming with Prof. Ian Ferguson, Georgia Institute of Technology for characterization of materials and device structure design. By combining Cermet's crystal growth technology with Cermet's high quality ZnO bulk substrates and thin films, we feel that ZnO based Spin LED's will be an ideal light source for defense and communications devices.

## **2. Objectives**

The fabrication of a spin Light Emitting Diode (spin LED) and the determination of maximum spin injection and polarization efficiency based on ZnO-GaN hybrid spin LED are the main objectives of Phase II work. Two different approaches will be exploited to achieve the desired goal. LED structures will be grown as described in figures 1a and 1b, The first approach is the growth of GaN based LED structure with transition metal doped ZnO as spin injector using MOCVD as illustrated in figure 1a. This objective will be explored by the researchers of

Cermet, Inc and Georgia Institute of Technology using state of the art MOCVD tools. The LED structure will be designed and fabricated based on quantum selection rules to have maximum spin injection and spin polarization efficiency. Spin injection and spin polarization efficiency will be measured for the grown LED structure. The growth of a GaN-ZnO based LED structure with transition metal doped ZnO as spin injector using MOCVD as depicted in figure 1b is the second approach to be explored. This task will be accomplished by the researchers of Cermet, Inc and Georgia Institute of Technology using state of the art MOCVD tool. Spin injection and polarization efficiency will be measured for the grown LED structure and the device fabrication process will be optimized. The successful results of these objectives will be utilized to identify the LED structure which provides highest spin injection and polarization efficiency and a spin LED will be fabricated.

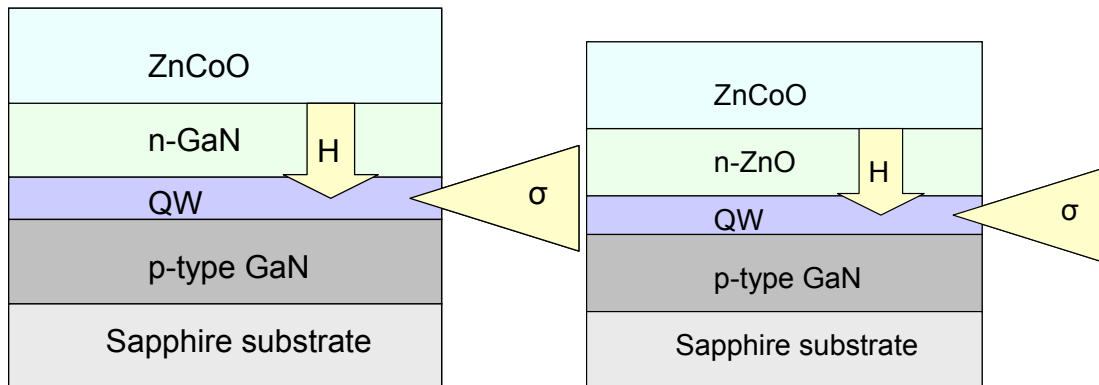


Figure 1a & b Proposed spin LED structures

### **3. Background**

#### **Bulk Growth Technology**

Cermet's crystal growth technology is a high-pressure induction melting apparatus, wherein the melt is contained in a water-cooled crucible. The heat source used during the melting operation is RF energy. Induced fields in the charge material produce eddy currents, which produce joule heating in the material until a molten phase is achieved. The highly refractory melt produced is contained in a cold wall crucible, such that part of a solid thermal barrier between the molten material and cooling fluid is of the same composition as the melt. The cooled material prevents the molten material from coming into direct contact with the cooling surface, which eliminates contamination from the crucible. This entire melting process is carried out in a controlled gas atmosphere ranging from 1 atm to over 100 atm, which prevents the evolution of volatile components, as well as the decomposition of some compounds into atomic species.

#### **MOCVD Technology**

For oxide film deposition, Cermet employs a Low Pressure Rotating Disk Reactor – Metal Organic Chemical Vapor Deposition (LP-RDR-MOCVD) system fabricated by Structure Materials Inc. Acetylacetonates will provide the starting materials for the growth of transition metal doped ZnO thin films. A radiative heater is used to heat the samples. The temperature, pressure, rotation, and mass flow rates are monitored and controlled by a computer. A carrier gas is used to carry reactants, in vapor form, from bubbler sources. Reactant sources and

delivery lines can be temperature controlled. The growth temperature can be varied from room temperature to approximately 1000°C.

#### **4. Status of the Effort**

During this research period of Phase 2 program, transition metal doped ZnO single crystals were grown by Cermet's patented melt growth technique. The grown crystals were characterized for crystal quality by X-ray diffraction. Optical measurements were carried out to find out the effect of dopants on the optical properties of ZnO single crystals. Raman spectra were taken for the transition metal doped ZnO single crystals and findings indicate good structural quality. EPR measurements were performed to find out the paramagnetic defects, impurities and to explore the local environment of the centre of its interactions. Co and Ni doped thin films were grown by Cermet's state of the art MOCVD technology. The growth parameters were optimized to grow high quality thin films. The grown films were characterized for quality and structure by X-ray diffraction and optical measurements. Magnetic measurements were recorded for the grown films. The results indicate room temperature ferromagnetism with Co and Ni doped ZnO thin films. n and p type GaN thin films were grown by Georgia Institute of Technology by the state of the art MOCVD technology. X-ray diffraction studies were performed to study the quality of the grown films. GaN LEDs have been fabricated. Electrical and optical characterizations indicate excellent electroluminescence and I-V characteristics. Co doped ZnO thin films were successfully deposited by MOCVD on MOCVD grown GaN without oxidizing GaN.

#### **5 Accomplishments**

##### **Growth**

Using Cermet's high pressure proprietary technique, we have melted boules of Mn and doped ZnO and obtained substrate crystals for nitride epitaxy. The grown single crystal wafers are shown in figure 2. Samples were cut from the crystals perpendicular to the crystallographic c-axis and double side polished. These substrates were polished to a RMS surface finish of approximately 7 angstroms. The crystals have excellent crystalline quality. The color of the crystals depends on the dopant material and the concentration of the dopant. Ni and Co doped ZnO thin films have been grown by MOCVD. Initial growth runs were performed on quartz and sapphire substrates. Later all the growth experiments were carried on sapphire and ZnO substrates. Acetylacetonate (acac) precursors were used as starting materials and oxygen gas was used as oxygen source. The sublimation temperatures of the precursors were calculated by heating them under argon atmospheres and the sublimation temperatures were listed in table 1. Ar gas was used as a carrier gas. The growth parameters were optimized by varying chamber pressure, flow rate of the carrier gas, temperature of the precursor bubbler and the reactor temperature. The dopant concentration has been changed by changing the bubbler temperature and the flow rate of the carrier gas. Figure 3 shows the picture of Ni doped ZnO film grown by MOCVD. The reactor temperature was maintained between 350-475°C. Films obtained have been of good transparency, clear and crack free. In addition, we have been able to calibrate our growth apparatus on a way that it is possible to obtain repeatability in the quality of the films. Most films have been grown on ZnO substrates as these are going to be the substrate of choice for final devices

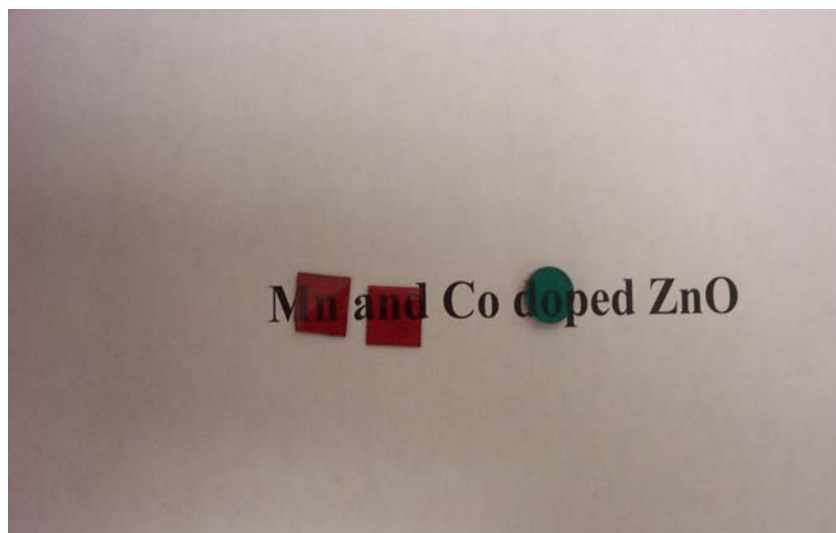


Figure 2 Mn and Co doped ZnO single crystal wafers

Precursor	Zn(acac)	Co(acac)	Ni(acac)
Sublimation Temperature (° C)	85	150-175	175-205

Table 1 Calculated sublimation temperatures of Metalorganic Precursors

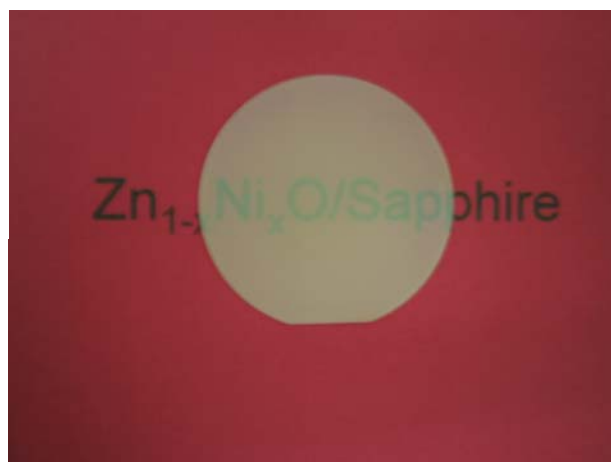


Figure 3 MOCVD grown ZnNiO thin film

### Characterization

#### X-ray Diffraction

High resolution XRD was performed on the single crystal samples using a Philips X'Pert PRO MRD 4-circle diffractometer.  $\omega$ -2 $\theta$  scans performed on both undoped and Mn, Co doped crystals showed that the as-grown material was completely oriented single crystal as no peaks attributable

to second phase formation were observed. Only c-axis (002) and (004) peaks from were visible as shown in figure 4.

The measured c-axis lattice parameter was 5.207Å for undoped sample, but increased with Mn incorporation to a value of 5.211Å at the 2.5% doping level. An increase in lattice parameter with Co dopant was also observed as shown in figure 5. Phi scans from the asymmetric reflections clearly revealed the 6-fold symmetry of the wurzite structure and thus *confirming any free Co or Mn or its oxide derivatives crystal*.

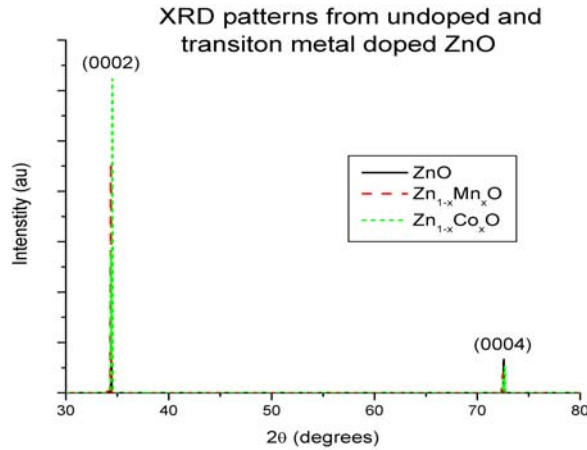


Figure 4 XRD patterns from undoped and CO, Mn doped ZnO

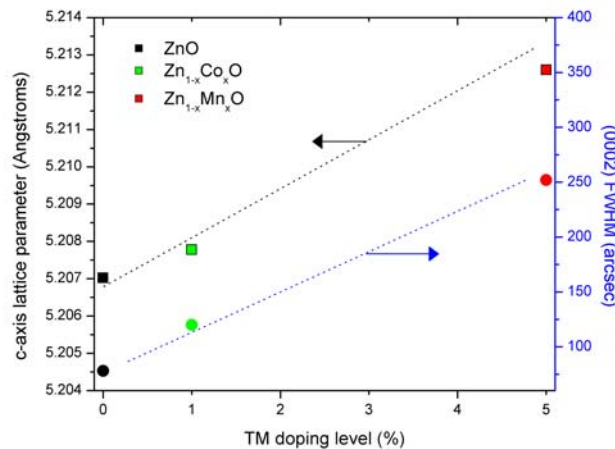


Figure 5 Lattice parameter values with dopant concentration of Mn and Co

The MOCVD grown films were characterized by X-ray diffraction for structure and quality. Co and Ni doped ZnO thin films show excellent crystalline quality and are single crystalline in nature. Figures 6 and 7 depict X-ray diffraction pattern of Co Ni doped ZnO thin films. As clear from the figure the films do not have any free Co Ni and its oxides. CoO precipitation have been observed on PLD grown Co doped ZnO films reported by Kim et al<sup>10</sup>.

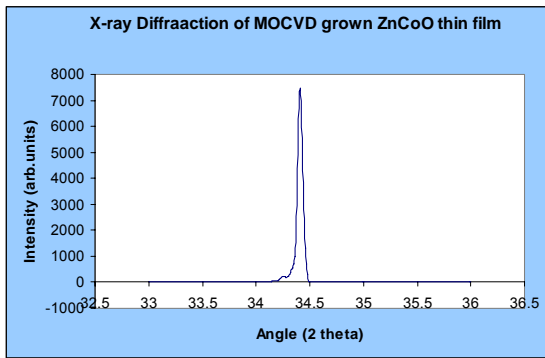


Figure 6

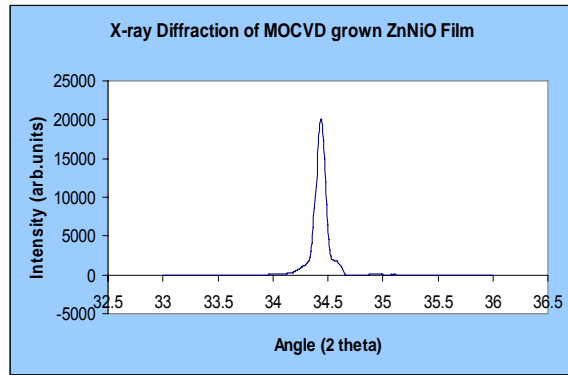


Figure 7

### Optical Characterizations

The most prevalent feature about the individual transparent crystals of the transition metal doped ZnO is the distinct, brilliant color with varying transition metal doping. The cobalt doped samples show a striking green color, which deepens with increasing cobalt concentration. Similarly, the Mn doped samples possess a range of reddish colors, from a pale orange for the samples doped at  $< 0.2\%$  Mn, to a deep red for samples doped at 3%. UV-visible transition measurements taken from these samples confirm that these trends are attributed to interatomic transitions within the divalent metal dopant atoms Figure 8 shows the transmission results of Mn doped ZnO bulk crystals. The undoped ZnO crystal shows a sharp absorption edge at 391.4nm (3.17eV). The absorption edge shifts nonlinearly from 500nm at 0.2% to 552.7 nm at 0.6% to 607.5 nm at 2.5% with increasing Mn concentration as shown in figure 10. Also it is evidenced from the figure 9 that there was no characteristic absorption from Mn and thus conforming a homogeneous crystal. The shift in absorption edge is shown in figure 10.

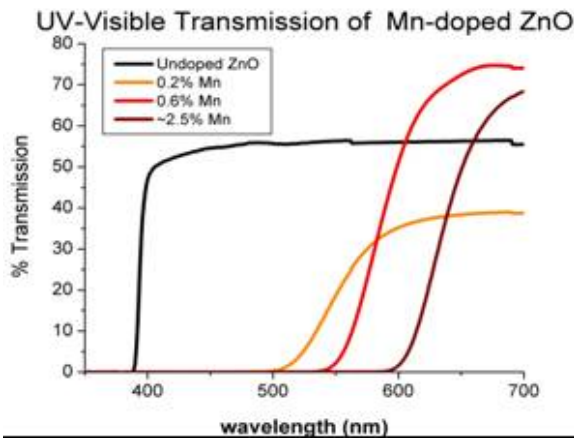


Figure 8 UV –Visible transmission spectrum of ZnMnO

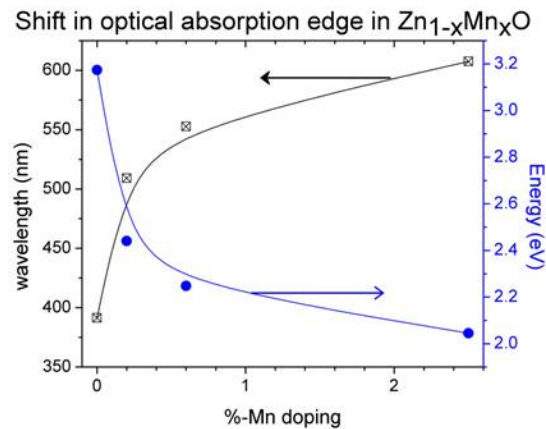


Figure 9 Absorption edge change with Mn doping

The UV-visible spectrum of Co doped ZnO single crystals shown is figure 10 The absorption edge increases with Co doping as clear from the figure.

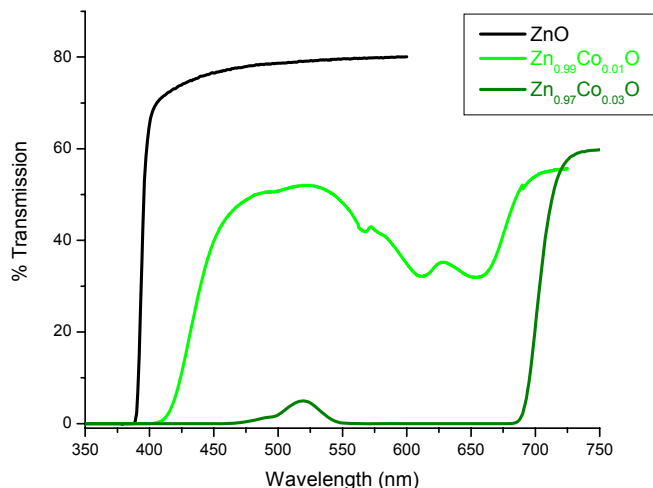


Figure 10 UV-visible spectrum of Co doped ZnO single crystal

Figure 11 shows AFM picture of Co doped ZnO thin film grown by MOCVD. AS seen from the picture the film shows uniform grain structure.

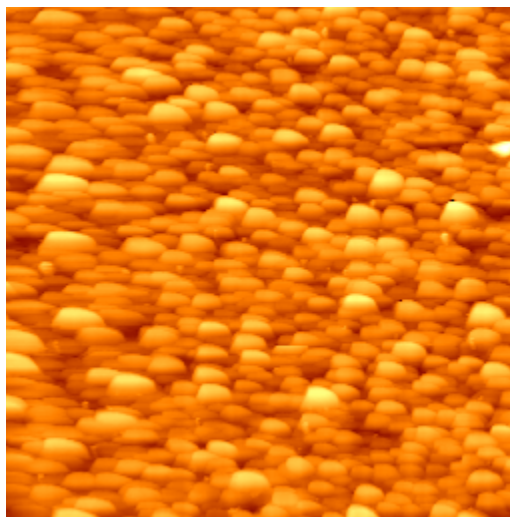


Figure 11 AFM picture of ZnCoO thin film

### Raman Spectroscopy of TM doped ZnO bulk crystals

Raman spectra are shown for varying concentrations of transition metal dopants in the  $Zn_{1-x}Mn_xO$  and  $Zn_{1-x}Co_xO$  systems in the figures 12 and 13. The scans for the undoped crystal are shown at the bottom of the graph; the other curves are shifted for clarity. In the undoped sample, the most prevalent feature are the lines at  $437\text{ cm}^{-1}$ , which corresponds to the  $E_2$  (high) mode and at  $332\text{ cm}^{-1}$  which correspond to a 2-phonon line. There is also a shoulder on the  $E_2$ (high) peak at  $407\text{ cm}^{-1}$ , which has been previously indexed as the  $E_1$ (LO) mode, and a smaller peak at  $202\text{ cm}^{-1}$  corresponding to twice the  $E_2$ (low) mode<sup>11</sup>. Upon Mn doping, the overall shape of the Raman spectrum changes, due to the loss of symmetry conservation leading to the appearance of ‘silent’ and mixed Raman modes from points off the center of the Brillouin zone<sup>12</sup>.

In  $Zn_{1-x}Mn_xO$ , these modes are particularly prevalent at  $522\text{ cm}^{-1}$  and  $580\text{ cm}^{-1}$ . The major peaks of the undoped ZnO lattice are still also visible, indicating that the structural quality is only slightly degraded. The  $Zn_{1-x}Co_xO$  shows a similar behavior, though the silent modes are less enhanced, and there is still a strong contribution from the  $437$  and  $332\text{ cm}^{-1}$  modes of the host lattice. Also, the dominant mode in the disordered region appears to be closer to  $550\text{ cm}^{-1}$  vice  $522$  or  $580\text{ cm}^{-1}$ . These findings are quite similar to reports of Raman spectra in  $Zn_{1-x}Co_xO$  which does exhibit the ferromagnetic behavior<sup>13</sup>.

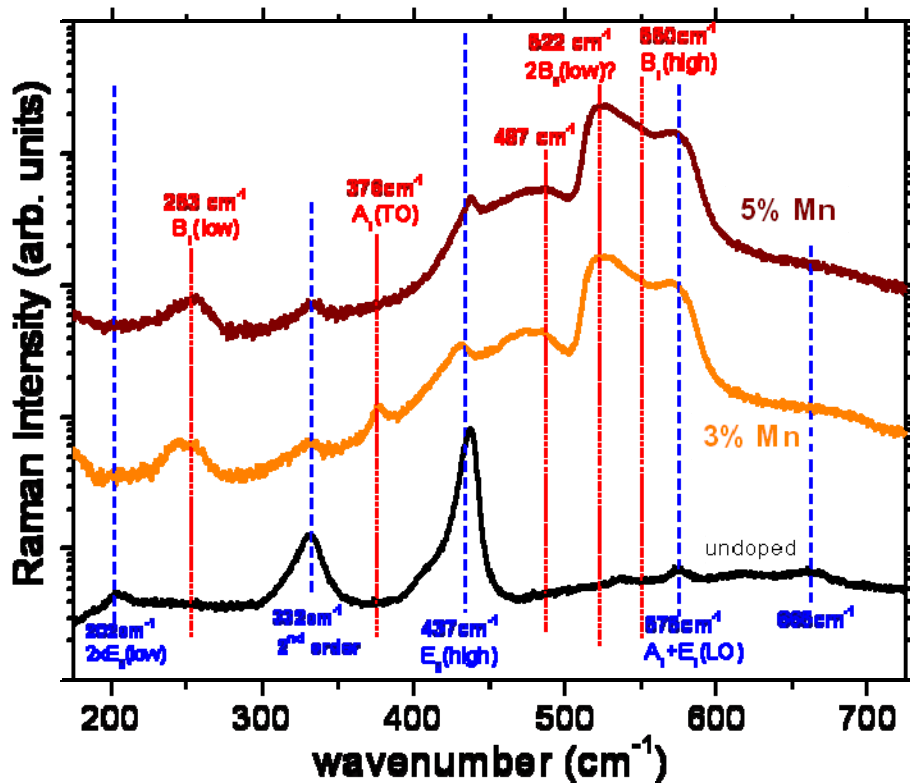


Figure 12 Raman spectra Mn doped ZnO bulk crystal

## Electron Paramagnetic Resonance Studies

### **EPR Results for ZnO:Mn 3% single crystals**

Electron paramagnetic resonance (EPR) is a highly sensitive technique for identifying paramagnetic defects and impurities. It can provide detailed insight on the local environment of the centre and its interactions. EPR Measurements at 9.5 GHz were made at temperatures below  $\sim 100\text{ K}$ . The resonant cavity Q factor was severely damped for higher temperatures due to the lossy component of the sample dielectric constant at 9.5 GHz. The 9.5 GHz EPR spectra for  $B$  parallel and perpendicular to the  $c$ -axis are shown in Figure 14. Comparison of the 0 and 90 Deg experimental spectra shows weak anisotropy. However, a more detailed examination of the wing regions for 0 Deg, as depicted in figure 15, shows evidence for further transitions. In the main central region the fit between experiment and simulation is reasonable, but not perfect. Likewise in Figure 15 there are discrepancies in the high field wing region. It should be noted that the Spin Hamiltonian (SH) given by A. Hausmann et al<sup>14</sup> is specified at room temperature, while the

measurements shown were performed at 11 K, small variations in both the ZFS and hyperfine terms are likely.

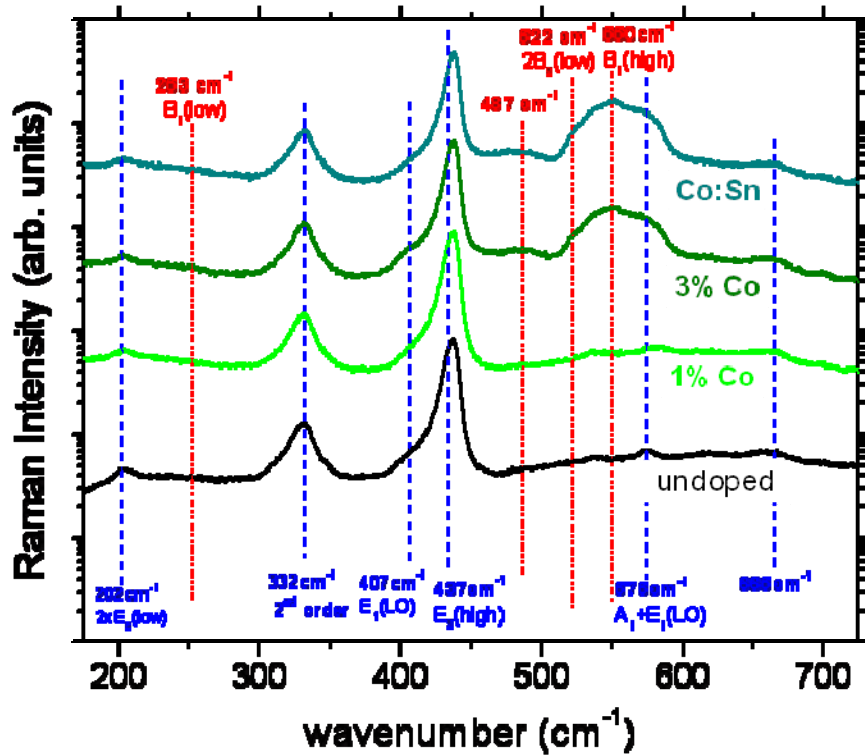


Figure 13 Raman spectra Co doped ZnO bulk crystal

These 9.5 GHz spectra also provide evidence for the presence of an additional broad underlying signal from the crystal. This can be seen by comparison the simulated to experimental spectra. Its presence is made clear in the 94 GHz B||c 5K spectra shown in Figure 16, particularly in the high power spectrum. The origin of this signal is unknown at present.

It is of potential interest to study the temperature dependence of the number of paramagnetic spins contributing to the observed spectra. This can be obtain by double-integrating the experimental spectra to determine the area under the absorption. The variation with temperature measured at 9.5 GHz is shown in Figure 17. Curie dependence is observed at low temperatures, but as the temperature is raised above  $\sim 50$  K the loss of intensity is far more rapid than predicted by the Curie law. This suggests either the onset of magnetic coupling or the onset of increased conductivity resulting in a decrease in the resonator Q. Since the Q does decrease though this region the later mechanism is more probable.

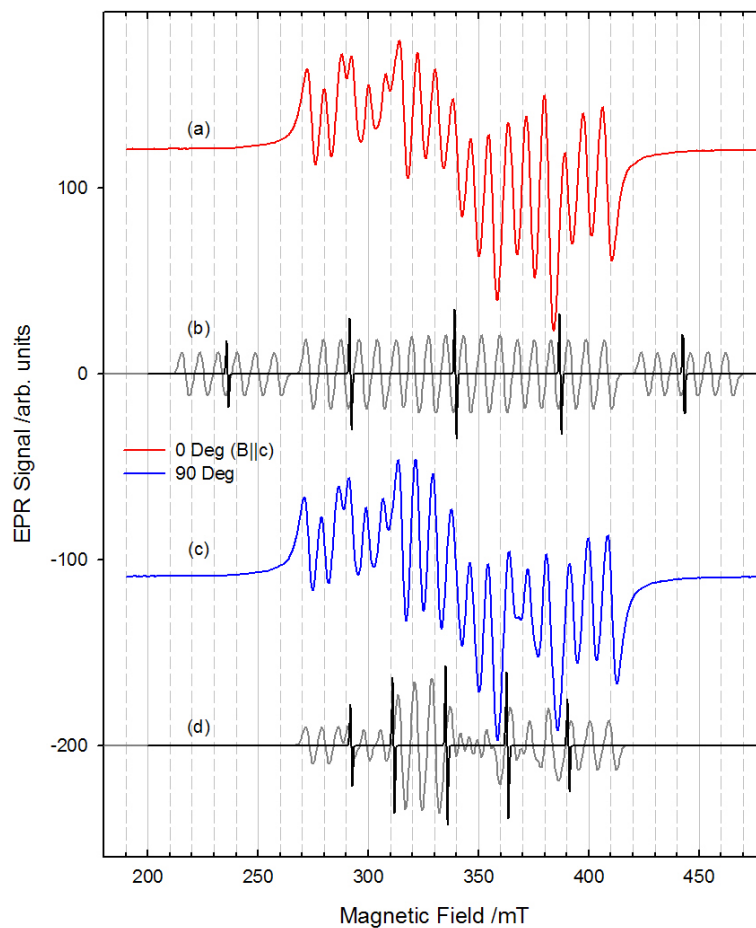


Figure 14 9.5 GHz spectra (a) 0 Deg (B||c) (b) simulation (grey), with no hyperfine (black) (c) 90 Deg (d) simulation (grey), with no hyperfine (black).

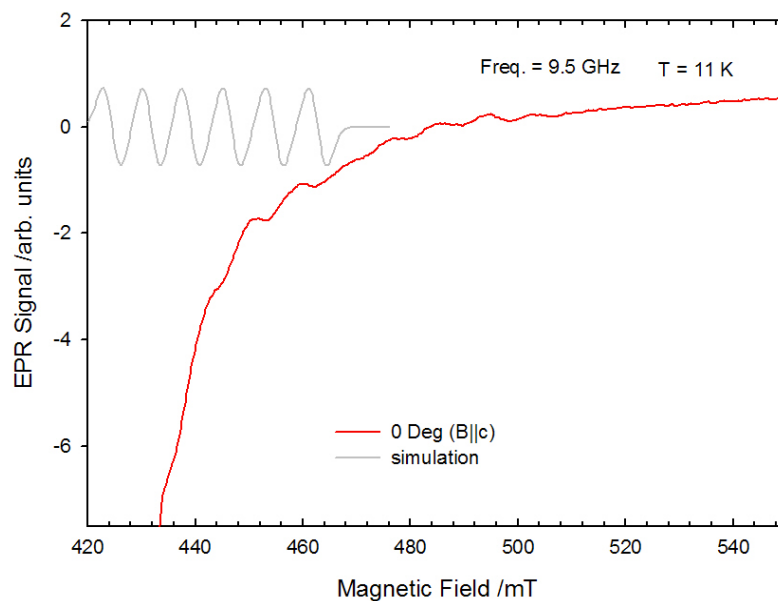


Figure 15 9.5 GHz spectra 0 Deg (B||c) and simulation (grey).

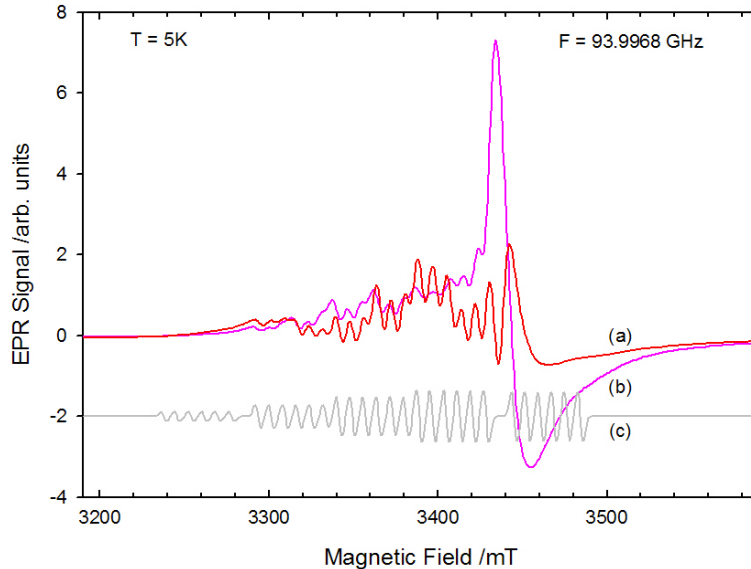


Figure 16 94 GHz spectra 0 Deg (B||c) (a) low power (red) (b) high power (pink) and (c) simulation (grey).

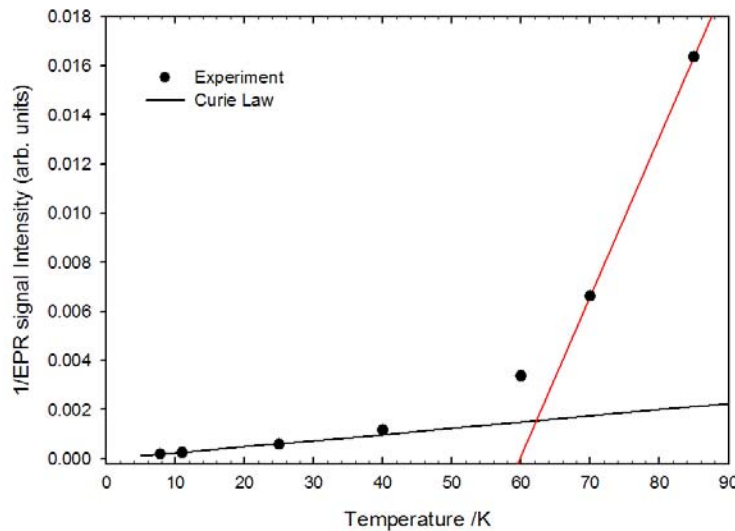


Figure 17 Inverse 9.5 GHz double-integrated EPR intensity versus temperature, experiment (solid black circles). Curie behaviour (black line), high temperature fit (red line).

### EPR Results for ZnO:Co 3% single crystals

Measurements at 9.5 GHz were made at temperatures below  $\sim 60$  K. The resonant cavity Q was observed to degrade for higher temperatures. The expected anisotropy was observed, as shown in Figures 18 and 19. No hyperfine splittings were resolved, but the variation in line width with angle is consistent with the hyperfine parameters as reported by T. Estle et al<sup>15</sup>. Additional lines are clearly visible in Figure 18. These are further examined in Figures 20 and 21, which also include the results of wider field range scans.

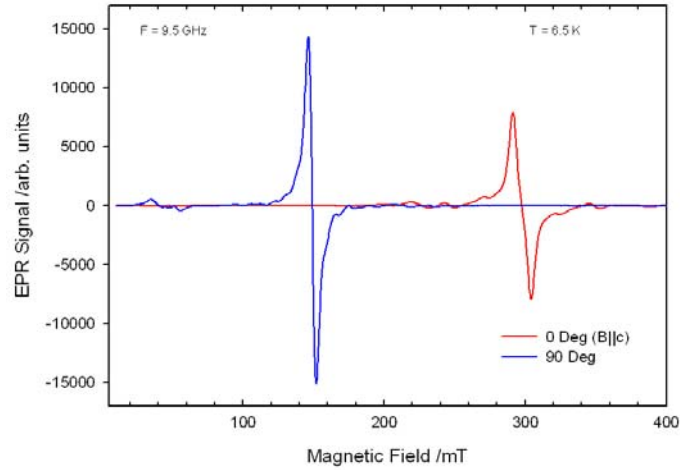


Figure 18 9.5 GHz spectra 0 Deg (B||c) (red) and 90 Deg (blue).

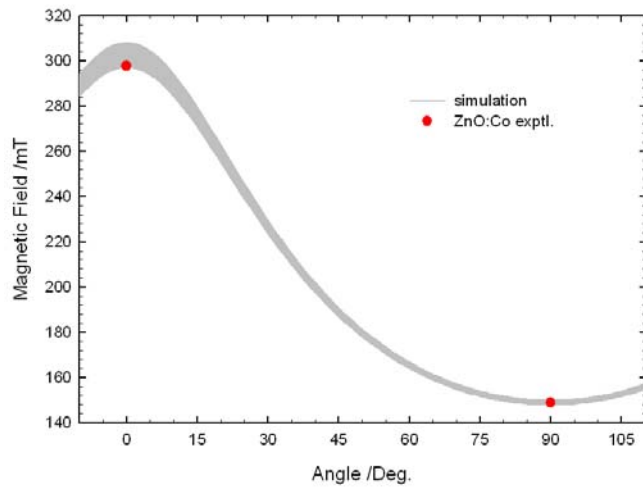
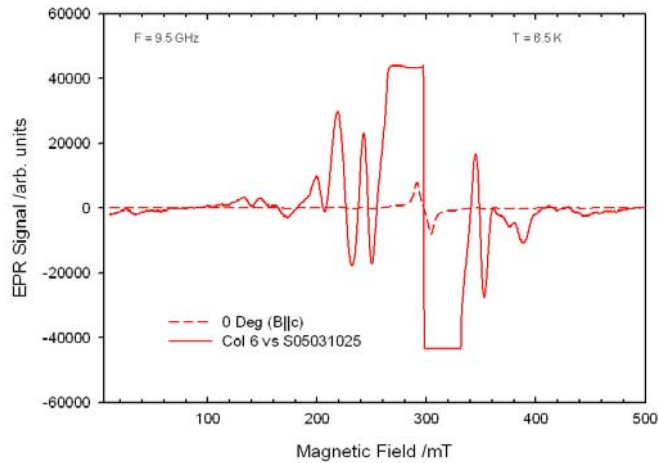


Figure 19 9.5 GHz simulated roadmap using Table II SH, exptl. positions (red).



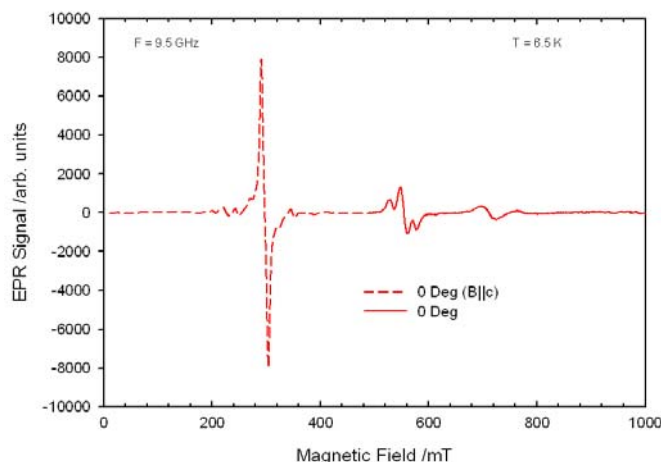


Figure 20 9.5 GHz spectra 0 Deg (B||c) top – expanded view of main line, bottom – expanded field range.

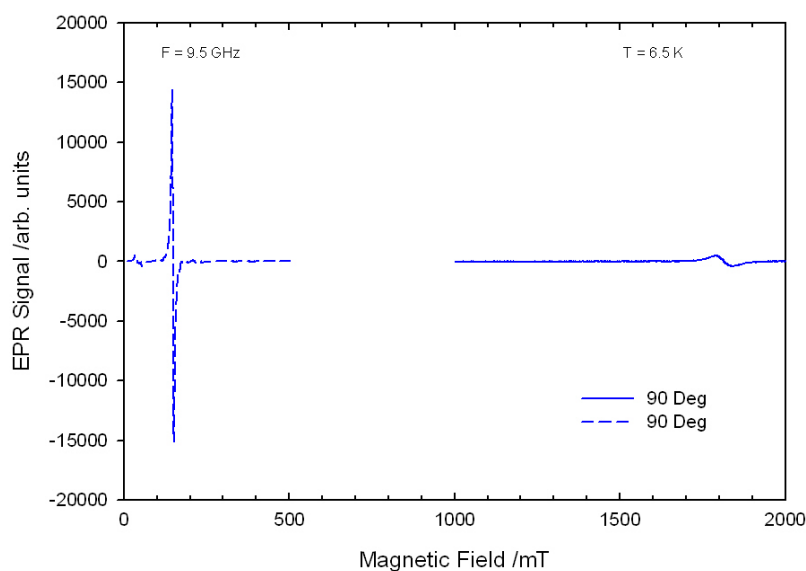


Figure 21 9.5 GHz spectra 90 Deg, expanded field range.

In principle high frequency measurements could simplify the interpretation of the 9.5 GHz spectra and allow an accurate determination of the ZFS term value. Spectra have been measured for B || c at both 94 and 188 GHz, as shown in Figure 22.

### **EPR Results for ZnO:Co,Sn single crystals**

The 9.5 GHz spectra are shown in Figure 23. These are similar to the Co doped spectra as shown in Figure 18, however, the intensity of the unidentified structure is greater for these samples. Likewise the wider field scan spectra shown in Figure 24 are similar, but not identical to those shown in Figure 20. Figure 25 shows the variation in the integrated intensity of the main EPR line as a function of temperature and can be compared to Mn case shown in Fig. 17.

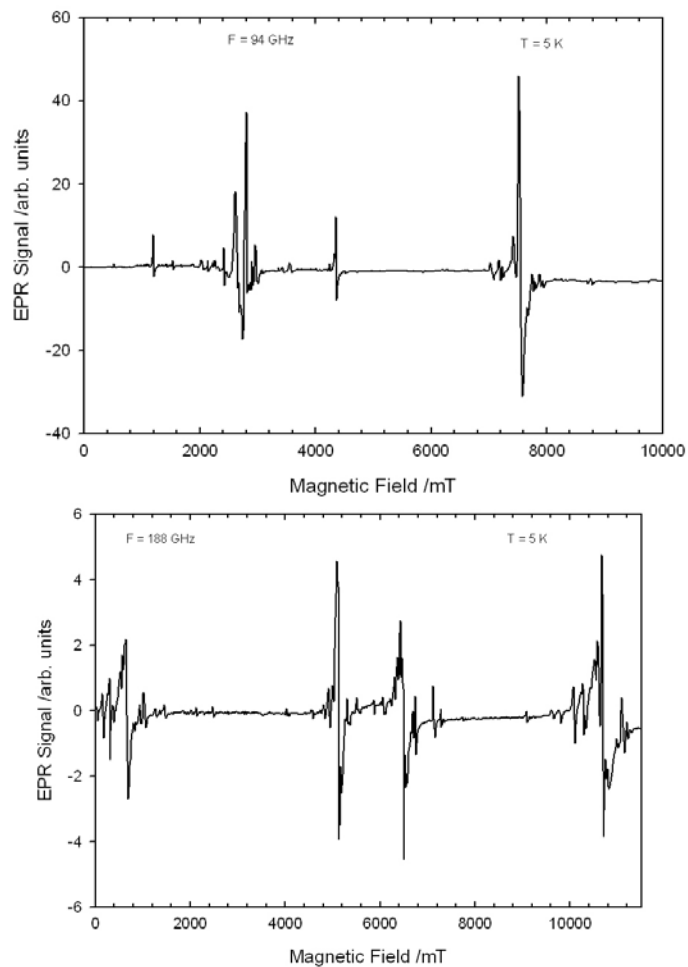


Figure 22 94GHz (top) and 188 GHz (bottom) EPR spectra for 0 Deg ( $B \parallel c$ ).

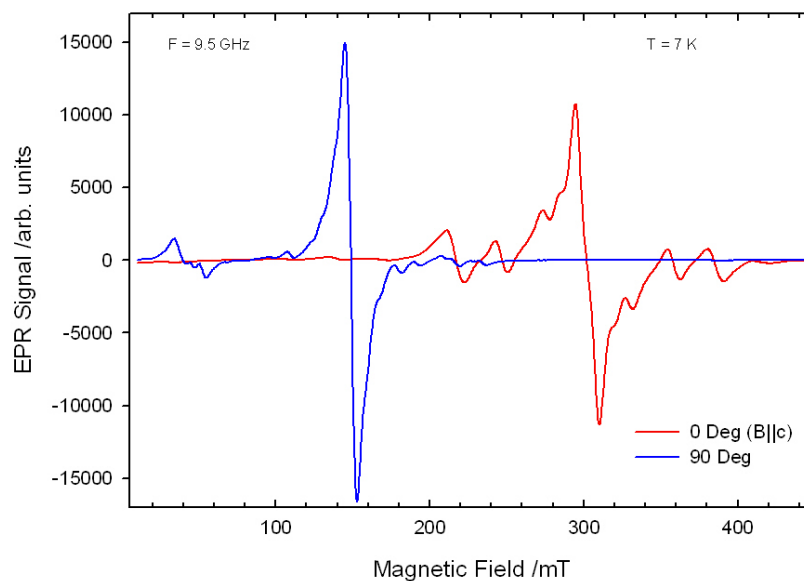


Figure 23 9.5 GHz spectra 0 Deg ( $B \parallel c$ ) (red) and 90 Deg (blue).

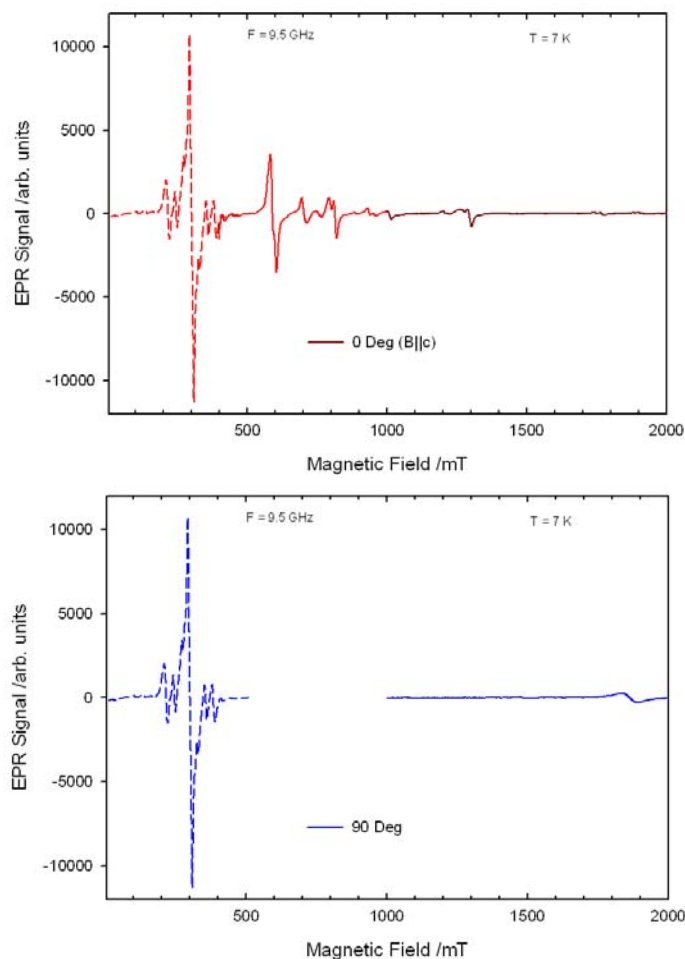


Figure 24 9.5 GHz spectra 0 Deg (B||c) top – expanded view of main line, bottom – expanded field range.

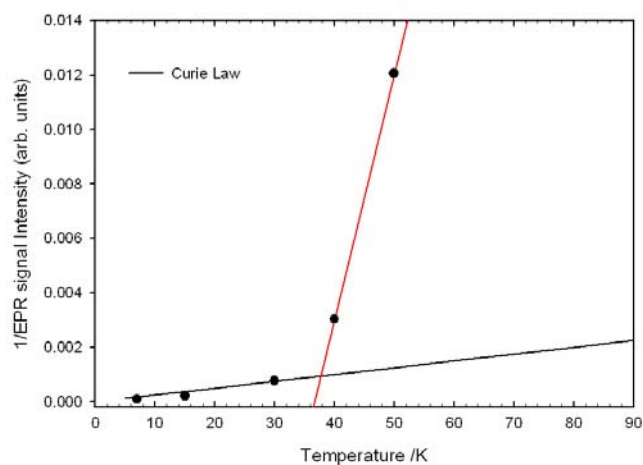


Figure 25 Inverse 9.5 GHz double-integrated EPR intensity versus temperature, experiment (solid black circles). Curie behaviour (black line), high temperature fit (red line).

EPR readily observes both  $\text{Mn}^{2+}$  and  $\text{Co}^{2+}$  in these crystals. The main features of the spectra are approximately reproduced by the published spin Hamiltonians. However, in the case of the Mn

doped crystals the  $M_S \pm 5/2$  transition groups were poorly resolved compared to the simulations and the exact values of the ZFS and hyperfine terms seem to be slightly different. In addition there is broad single line resonance superimposed on the Mn signal, this is more clearly seen in the 94 GHz spectrum. The origin of the signal is currently unknown.

The Co doped and Co, Sn doped crystals show similar features, the main line is in approximate agreement with the previously published SH. The high concentration of Co broadens the line preventing the hyperfine structure from being resolved. For both crystals there is a complex set of unexplained transitions extending over a very wide field range in the 9.5 GHz spectra. The 94 and 188 GHz measurements have the potential to accurately determine the ZFS term for the  $S = 3/2$   $\text{Co}^{2+}$  centres, however, initial attempts to fit these spectra have not been successful.

For the three crystals studied the 9.5 GHz measurements showed the onset of loss mechanisms in the samples for temperatures greater than  $\sim 50$ -100 K giving a degradation of the resonant cavity Q. The most probably mechanism is the ionisation of carriers making the samples conducting at higher temperatures.

Measurements on lightly doped crystals,  $\sim 0.01\%$ , would likely allow the spin Hamiltonian parameters of the isolated centres to be accurately determined over the temperature range of interest. The additional lines seen in the Co doped samples are of interest, these may arise from cluster centres, and a study of crystals with different doping levels may allow this proposal to be tested.

### **Magnetic Measurements**

Magnetic property measurements were performed with a VSM and SQUID. Figure 26 shows the magnetization vs. applied field plot for the Ni and doped ZnO thin films grown by MOCVD at room temperature. Figure 26 clearly shows that room temperature ferromagnetism. Also from the figure, it is clear that no dia or paramagnetic behavior is observed which indicates there is no ferromagnetic clustering or precipitation in the film.

### **GaN Growth and Characterization for Light Emitting Diodes (LEDs)**

Gallium Nitride (GaN) based materials with bandgaps ranging from 0.76 eV to 6.20 eV has become very important for many optoelectronic applications. GaN-based light emitting diodes (LED) are promising devices for use in solid state lighting applications as well as spin-polarized LEDs. The prediction and subsequent experimental verification that GaN-based diluted magnetic semiconductors exhibit room temperature ferromagnetism have led to a great deal of work in the area of GaN-based materials for use in spintronic devices<sup>16,17</sup>. However, a detailed understanding of GaN growth, characterization, and basic device structures is necessary in order to realize the potential of this material and others similar to it.

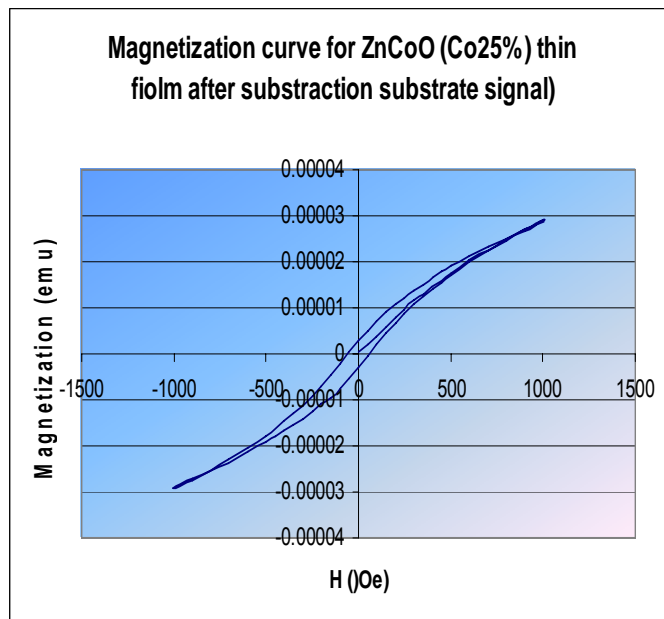
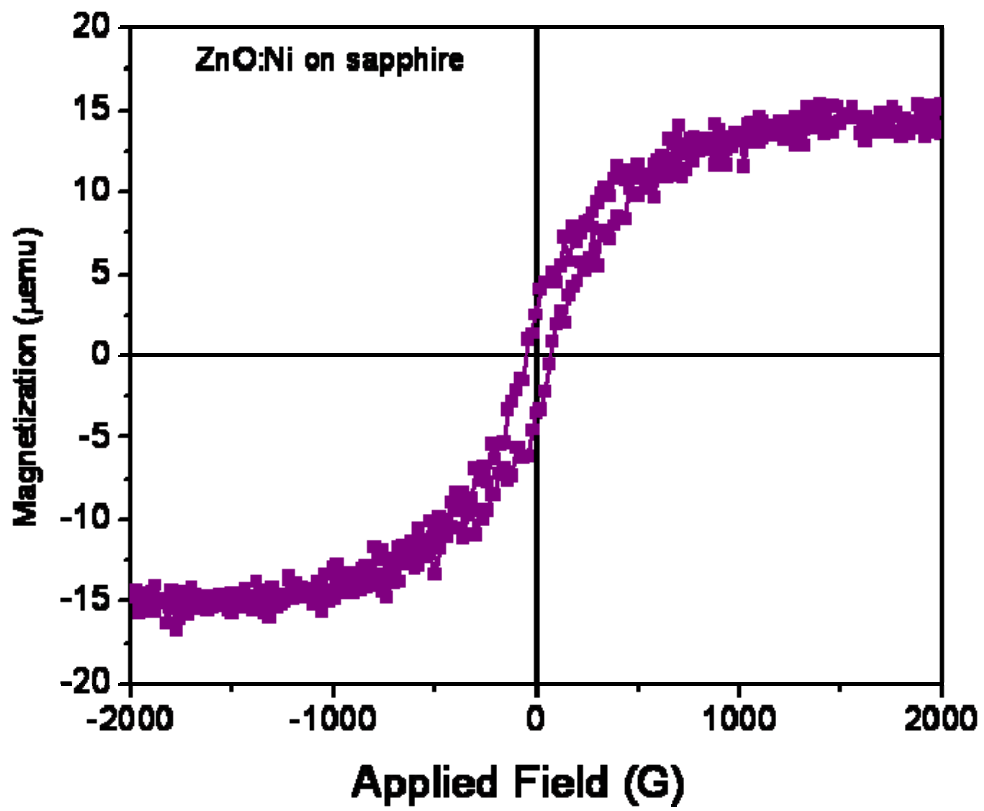


Figure 26 Magnetization curve for ZnNiO and ZnCoO

Metal organic chemical vapor deposition (MOCVD) is a widely-used growth technique for compound semiconductors in optoelectronic applications. In this work, a highly modified vertical injection MOCVD system was used to grow undoped, n-type, and p-type GaN on c-plane sapphire substrates for use in LED structures. Specifically, GaN-based p-i-n structures and quantum well structures were grown for use with ZnO-based DMS spin injection layers to create spin-LEDs.

Undoped GaN layers were grown using trimethyl gallium (TMGa) and  $\text{NH}_3$  as the precursors for Ga and N, respectively. A low temperature GaN buffer layer was grown on the c-plane sapphire substrate in order to relieve the strain caused by the large lattice mismatch between GaN and sapphire. High quality undoped GaN was then grown on the buffer layer. X-ray diffraction (XRD) and Raman spectroscopy were used to evaluate crystalline quality and structural properties. A typical XRD  $\theta$ - $2\theta$  scan of an undoped GaN layer grown on sapphire is shown in Figure 27. Crystalline quality is measured by peak intensity and by full width at half maximum (FWHM). Absence of second phases also indicates good crystal quality.

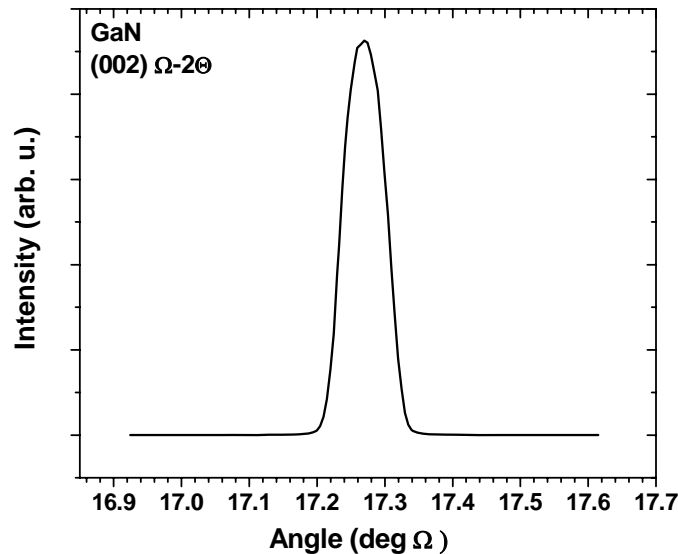


Figure 27.  $\Omega$ - $2\theta$  scan of an undoped GaN epilayer.

Device structures require the growth of reproducible, high quality n-type and p-type GaN in addition to undoped GaN films. In this work, n-type GaN was obtained by using Si as the n-type dopant with  $\text{SiH}_4$  as the precursor. Hall effect measurements were used to verify Si incorporation and to obtain carrier concentrations of the n-type films.

P-type GaN was obtained using Mg as the dopant with bis-cyclopentylidienyl magnesium as the precursor. P-type doping of GaN also requires an activation step. Post-growth annealing is typically done in a hydrogen-free atmosphere in order to break the Mg-H bonds that form during MOCVD growth. Reports also suggest that annealing in an atmosphere containing oxygen serves to increase the concentration of Mg that is activated in the p-type GaN layer<sup>18,19</sup>. Hall Effect measurements were used to verify activation of Mg and to obtain carrier concentrations of the p-type GaN films. Figure 28 shows PL data for Si doped GaN film.

Photoluminescence (PL) is also used to observe electronic defects in the material. Excitation at an energy less than the bandgap energy can reveal sub-bandgap states caused by dopant incorporation or intrinsic defects in the material. While dopant incorporation tends to degrade the structural properties of the films, good crystalline quality is imperative for proper device functionality. XRD and Raman spectroscopy were used to verify crystalline quality of the doped GaN epilayers.

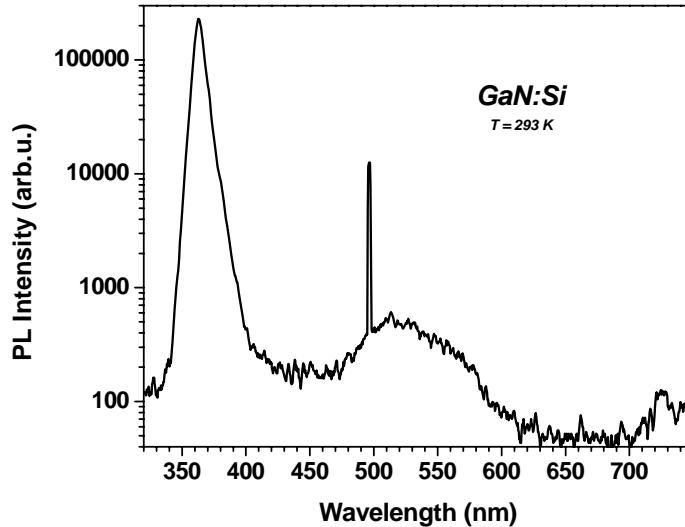


Figure 28 PL data for Si doped GaN film grown by MOCVD

First, basic p-i-n structures were grown and investigated for electrical and optical properties. A typical I-V curve of a GaN-based p-i-n junction LED is shown in Figure 29 below. This device shows a rectifying I-V characteristic with a turn-on voltage of roughly 5V. Figure 30 shows a photo of the device operating in the forward active region. The device shows strong light emission in the visible region. The electroluminescence response of this same device is shown in Figure 31. Note the high intensity and the single emission peak centered around 420nm. Indium can also be used in GaN-based quantum well structures to facilitate more efficient recombination. However, this leads to several growth problems that must be solved. It is important that thickness and In incorporation be uniform across the wafer. In order to achieve this, it is often necessary to create a temperature gradient across the wafer during growth. This allows for uniform incorporation of In across the wafer and for changes in cracking efficiency in areas where more or less of the precursors may reach the surface, leading to a uniform growth rate and thus uniform thickness. Indium incorporation is most often obtained from XRD results since the incorporation of In causes a shift in the (002) GaN peak and the magnitude of this shift is proportional to the concentration of In in the film. A ferromagnetic spin injector can be added to the structures mentioned above to create a spin-polarized LED. Both GaN and ZnO-based DMS are predicted to show room temperature ferromagnetism, making them ideal for room-temperature spin-LEDs. Though much work remains to be done to integrate these materials into

a single functional device, the study of GaN growth and its use in LED structures has provided knowledge that will no doubt be useful in solving these problems.

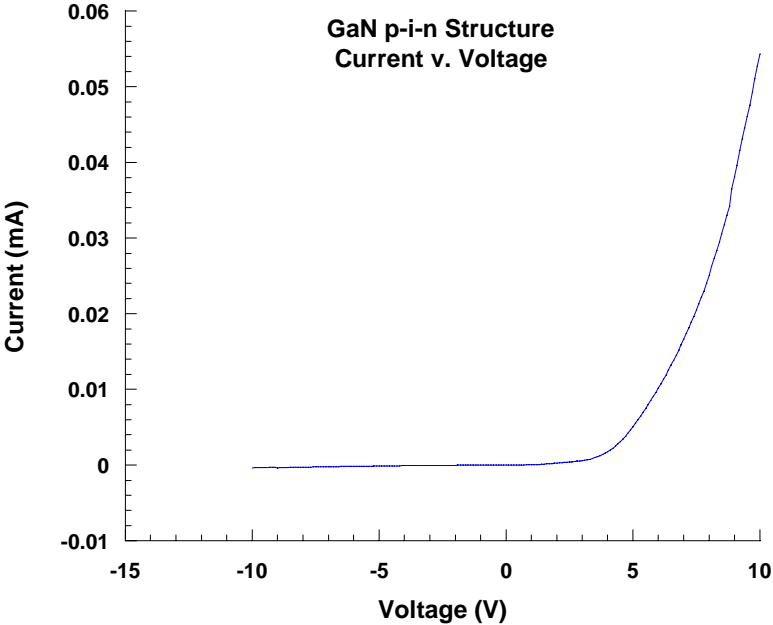


Figure 29. I-V Curve of a typical GaN-based LED.

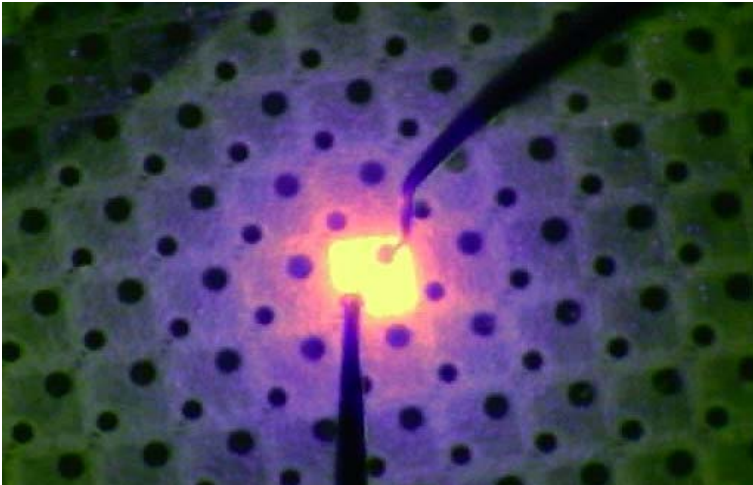


Figure 30. Photo of a GaN-based LED grown by MOCVD and biased in the forward active region.

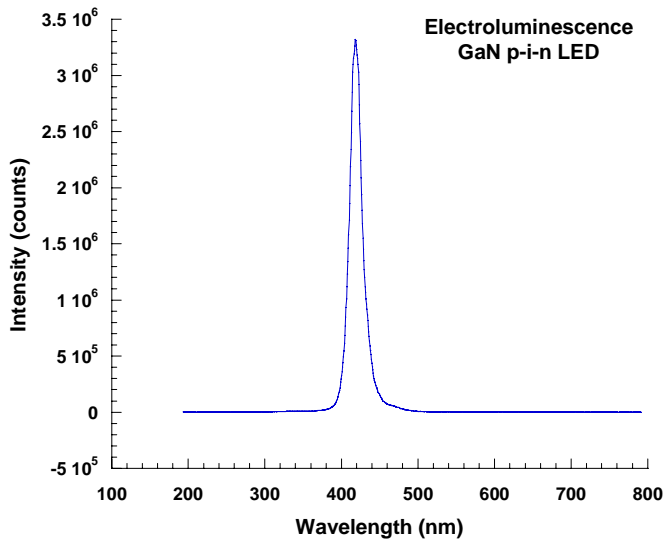


Figure 31. EL response of GaN-based p-i-n LED grown by MOCVD. The emission wavelength centers around 420nm.

### Growth of ZnO on GaN

Georgia Institute of Technology produced GaN thin film on sapphire substrates and Cermet, Inc deposited Co doped thin ZnO thin films on top GaN. The initial experiments were performed to avoid oxidation Gallium in GaN. The growth parameters were optimized in order to have Co doped ZnO with oxidizing GaN. Figure 32 and 33 show XRD pattern and SIMS measurements and confirm the presence of ZnCoO and GaN.

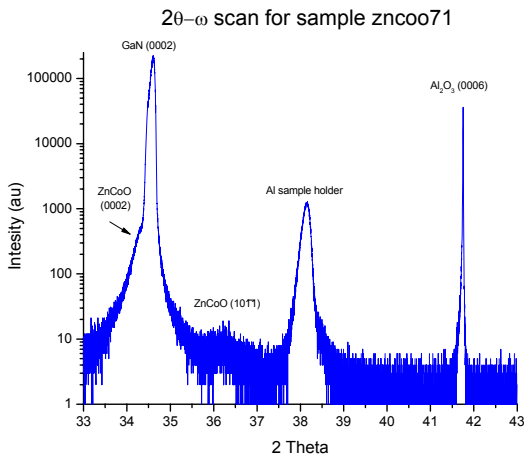


Figure 32 XRD pattern of ZnCoO/GaN/Sapphire

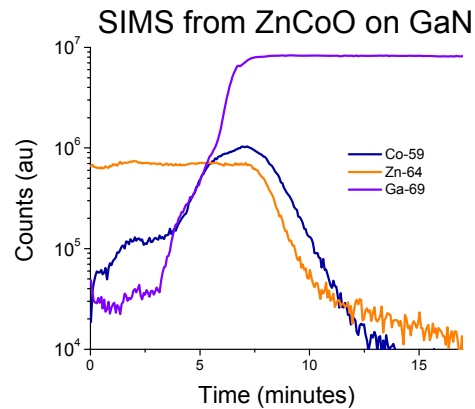


Figure 33 SIMS pattern of ZnCoO/GaN/Sapphire

### Growth of p-GaN-n-ZnNiO Hybrid LED

p-GaN thin films were grown on sapphire substrate by the researchers of Georgia Institute of Technology. N-ZnNiO thin films were deposited on p-GaN by Cermet and the electrical properties were studied. Figure 34 shows I-V curve of p-GaN-n-ZnNiO hybrid diode. As is clear from the figure, the diode shows rectification.

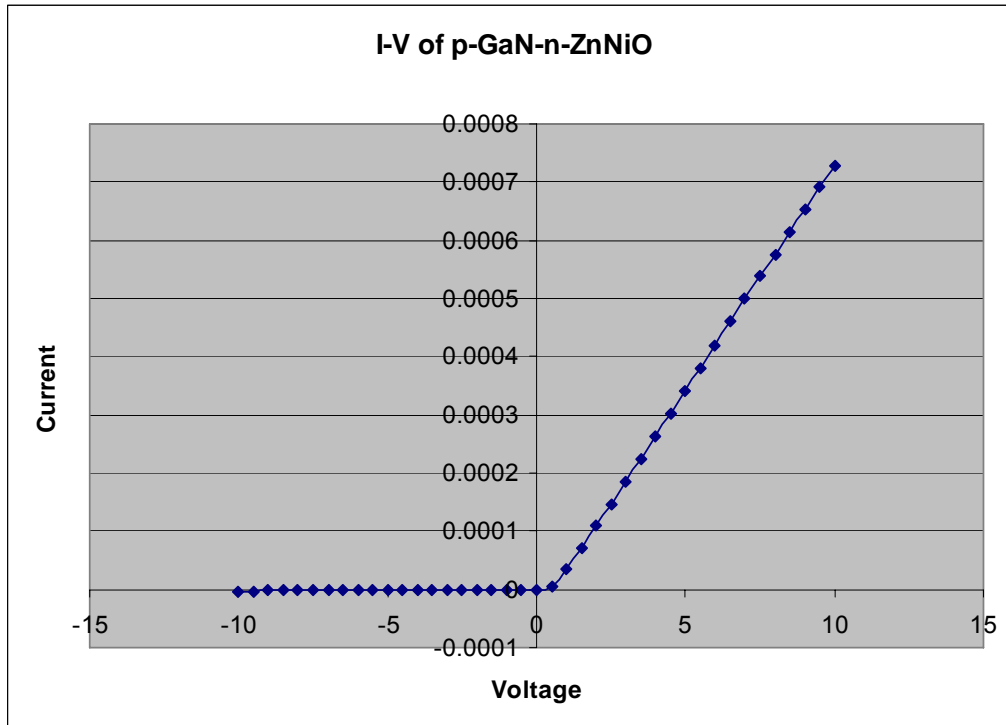


Figure 34 I-V characteristics of hybrid diode

### Summary

Based on the results of this period, we have shown:  
Successful growth of transition metal doped ZnO single crystals;  
Successful growth of Co and Ni doped ZnO thin films;  
Structural and optical Characterization of Grown single crystals and thin films;  
Raman and EPR characterization of TM doped ZnO;  
Magnetic characterization of TM doped ZnO;  
Ferromagnetism at room temperature;  
Successful growth of GaN on sapphire for LED structure;  
Successful growth of p and n type GaN;  
Fabrication and demonstration of GaN LEDs;  
Successful growth of ZnCoO on GaN;  
And the fabrication GaN-ZnNiO hybrid diode and rectification.

## **6. People involved in this work**

Dr. Varatharajan Rengarajan	Cermet, Inc
Jeff Nause	Cermet, Inc
Bill Nemeth	Cermet, Inc
Prof. Ian Ferguson	Georgia Institute of Technology
Matt Kane	Georgia Institute of Technology
William Fenwick	Georgia Institute of Technology
Nola Li	Georgia Institute of Technology

## **7. Participation**

Based on the results obtained during this research period of work following publications / presentations were made.

### 1. Prospects of ferromagnetism in Bulk crystals of TM doped ZnO

Jeff Nause

AFOSR Wide band gap ferromagnetic semiconductors workshop, Edinburgh, Scotland, 15-19 May 2005

### 2. Magnetic and optical properties of single crystals of transition metal doped ZnO

M.H.Kane, W.E.Fenwick, M.Strassburg, B.Nemeth, R.Varatharajan, C.R.Vestal, Z.J.Zhang, J.Nause, C.J.Summers, and I.T.Ferguson

E-MRS 2005 Spring Meeting, Strasbourg, France May31 – June 3 2005

### 3. Epitaxial growth and characterization of transition metal doped ZnO

thin films for spintronics applications

Varatharajan Rengarajan, Matt Kane, Ian Ferguson and Jeff Nause

16<sup>th</sup> American Conference on Crystal Growth, Big Sky, MY July 10-15 2005

### 4. Growth and ferromagnetic studies on bulk single crystals and MOCVD grown thin films of transition metal doped ZnO”

Varatharajan Rengarajan<sup>1</sup>, Matt Kane<sup>2</sup>, Nola Li<sup>2</sup>, Will Fenwick<sup>2</sup>, Ming Pan<sup>1</sup>, Bill Nemeth<sup>1</sup>, Ian Ferguson<sup>2</sup> and Jeff Nause<sup>1</sup>

Presented at “6<sup>th</sup> International symposium on blue laser and light emitting diodes” held at Montpellier, France between May 15-19 2006

### 5. W. E. Fenwick, M. H. Kane, M. Strassburg, B. Nemeth, R. Varatharajan, C. R. Vestal,

Z. John Zhang, J. Nause, C. J. Summers, and I. T. Ferguson, “Magnetic and optical

Properties of single-crystal transition metal-doped ZnO”, Presented at the Materials

Research Society Fall Meeting, Boston, MA, Dec. 2005

### 6. M. H. Kane, W. E. Fenwick, R. Varatharajan, M. Strassburg, B. Nemeth, D. J. Keeble,

H. El-Mkami, G. M. Smith, J. Nause, C. J. Summers, and I. T. Ferguson, “Transition

metal-doped ZnO: a comparison of optical, magnetic, and structural behavior of bulk and thin films”, Presented at Chinese Physics 2006

### 7. Varatharajan Rengarajan, Ming Pan, Matt Kane, Nola Li<sup>2</sup>, Will Fenwick<sup>2</sup>, Ian

Ferguson and Jeff Nause “ZnO for spintronics”, To be presented at 4<sup>th</sup> International

Workshop in ZnO and related materials, Giessen, Germany

8. M. H. Kane, W. E. Fenwick, R. Varatharajan, M. Strassburg, B. Nemeth, D. J. Keeble, H. El-Mkami, G. M. Smith, J. Nause, C. J. Summers, and I. T. Ferguson, "Transition metal-doped ZnO: a comparison of optical, magnetic, and structural behavior of bulk and thin films", Submitted to SPIE Photonics West 2007

## **8. References**

1. C. Kligshirn, Phys. Status Solidi B **71**, 547 (1975).
2. *Numerical Data and Fundamental Relationships in Science and Technology*, Vol. 17, Springer-Verlag, Berlin, 1982.
3. K.J.Kim and Y.R.Park, Applied physics Letters 78, 475 (2001)
4. S.Chichibu, T.Azuhata, T.Sota and S.Nakamura, J.Appl. Phys. 79, 2784 (1996)
5. J. Nause and G. Agarwal, "A New Approach to Growth of Bulk ZnO Crystals for Wide Bandgap Applications," Materials Research Society - Spring 1998 Meeting, San Francisco, CA
6. T.Fukumura, Z.Jin, A.Ohtomo, H.Koinuma and M.Kawasaki, Applied Physics Letters 75 1999 3366
7. T. Fukumura, Z.Jin, M.Kawasaki, T.Shono, T.Hasegawa, S.Koshinara and H.Koinuma Applied Physics Letters 78 2001 958
8. Z.K.Tang, P.Yu, G.K.L.Wong, M.Kawasaki, A.Ohtomo, H.Koinuma and Y.Segawa Solid State Communications, 103 1997 459
9. K.Sato and H.K.Yoshida Physica E 10 2001 251
10. J.H.Kim, K.Kim, D.Kim, Y.Ihm, W.K.Choo, Journal of European Ceramic Society 24 2004 1847
11. J. M. Calleja and M. Cardona, Physical Review B 16 (1977) 3753.
12. F. J. Manjon, B. Mari, J. Serrano, and A. H. Romero, Journal of Applied Physics 97 (2005) 053516.
13. N. Hasuike, H. Fukumura, H. Harima, K. Kisoda, H. Matsui, H. Saeki, and H. Tabata, Journal of Physics: Condensed Matter 16 (2004) S5807.
14. A. Hausmann and H. Huppertz, J. Phys. Chem. Solids **29**, 1369 (1968).
15. T. Estle and M. De Wit, Bull. Am. Phys. Soc. **6**, 445 (1961).
16. T. Dietl, H. Ohno, F. Matsukura, J. Cibert, and D. Ferrand, "Zener Model Description of Ferromagnetism in Zinc-Blende Magnetic Semiconductors," *Science*, vol. 287, pp. 1019-1022, 2000.
17. M. H. Kane, M. Strassburg, W. E. Fenwick, A. Asghar, and I. T. Ferguson, "The Growth and Characterization of Ferromagnetic Wide Bandgap Materials for Spintronic Applications," *International Journal of High Speed Electronics*, in press.
18. Y. Gong, Y. Gu, Igor L. Kuskovsky, G.F. Neumark, J. Li, J.Y. Lin, H.X. Jiang, A. Asghar, and I. Ferguson in *Non-Equilibrium Acceptor Concentration in GaN:Mg Grown by Metalorganic Chemical Vapor Deposition*, edited by H. Ng, M. Wraback, K. Hiramatsu, and N. Grandjean (Mater. Res. Soc. Symp. Proc. 798, Boston, MA, 2003) pp. Y5.16
19. Y.J. Lin, Appl. Phys. Lett., **84** (15), 2760, (2004).